

Supporting information for:

**Organic radical compound and carbon nanotube composites
with enhanced electrical conductivity towards high-
performance p-type and n-type thermoelectric materials**

Yanzhao Wang,^{ab} Zhanhua Chen,^a Hongfeng Huang,^a Dagang Wang,^a Danqing Liu^{*a} and Lei Wang^{*ab}

a. Shenzhen Key Laboratory of Polymer Science and Technology, College of Materials Science and Engineering, Shenzhen University, Shenzhen, 518060. China. E-mail: dqliu@szu.edu.cn, wl@szu.edu.cn.

b. Key Laboratory of Optoelectronic Devices and Systems of Ministry of Education and Guangdong Province, College of Optoelectronic Engineering, Shenzhen University, Shenzhen 518060, China.

Chemicals and materials

All chemical reagents were purchased from Energy Chemical Co., Ltd. and used without further treatment unless otherwise noted. SWCNTs (diameter: 1–2 nm, purity: >95.0 wt%) were purchased from XFNANO Materials Technology Co., Ltd (Nanjing, China). Anhydrous chlorobenzene and other chemical solvents, including ethanol, dichloromethane, acetone and isopropanol, were used as received without further treatment.

Preparation of NDI-0, NDI-1 and NDI-2

The diimides **NDI-0** was prepared by direct condensation of naphthalene dianhydride with the appropriate amine. Accordingly, a mixture of 1,4,5,8-naphthalenetetracarboxylic acid anhydride (1.34 g, 5.00 mmol), n-hexylamine (30 mmol), and zinc acetate (50 mg) in 15 mL quinoline was heated at 140–150 °C for four hours. The mixture was cooled and diluted with several volumes of methanol. The resulting slurry was filtered; the collected solid washed with methanol and dried in air to achieve the desired product **NDI-0**. Similarly, naphthalenediimide derivatives **NDI-1** and **NDI-2** could be obtained respectively by heating naphthalene-1,4,5,8-tetracarboxylic dianhydride with 1 equiv each of 4-amino-TEMPO and hexylamine or 2 equiv of 4-amino-TEMPO in N,N-dimethylacetamide (DMA) with acetic acid for several hours. The reaction mixture was then concentrated under reduced pressure to give a crude product, which was purified by column chromatography (Al_2O_3 , dichloromethane) and recrystallization from diethyl ether/dichloromethane.

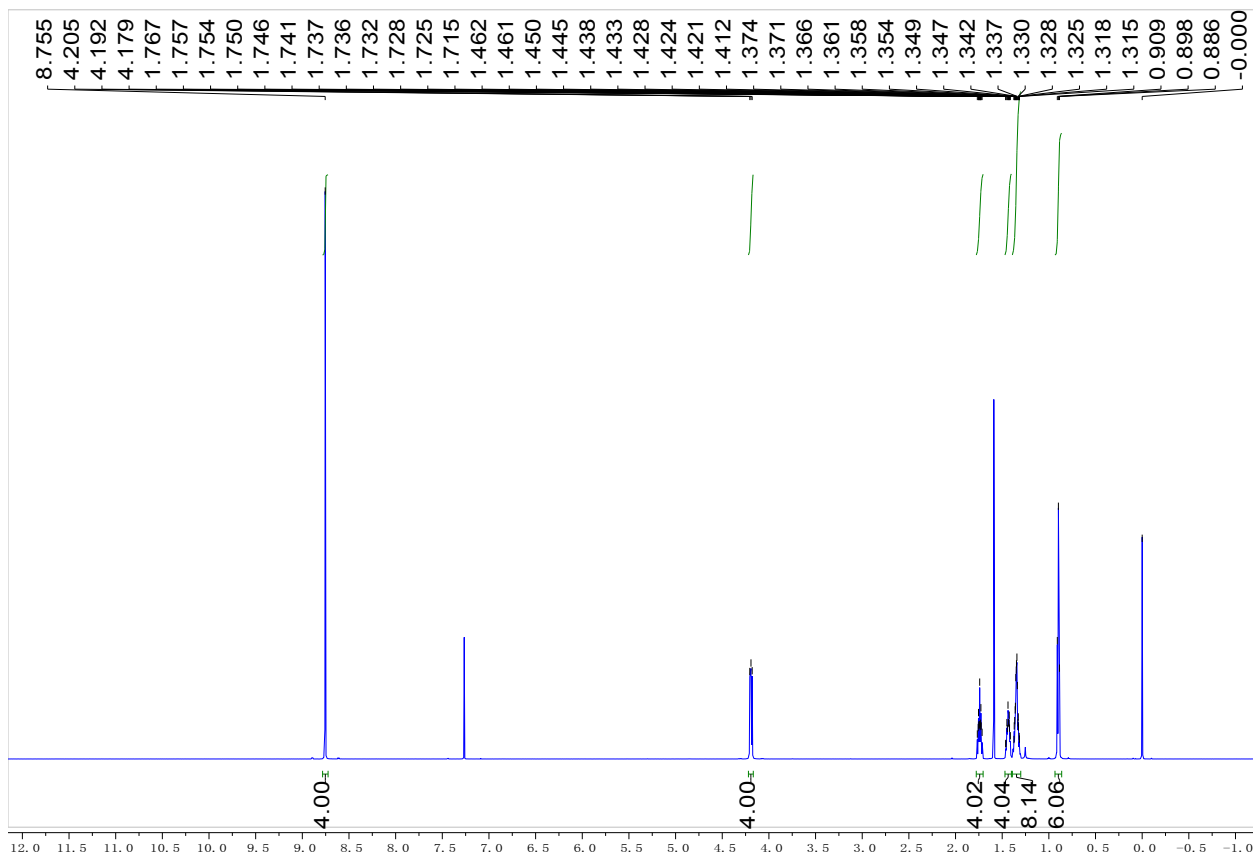
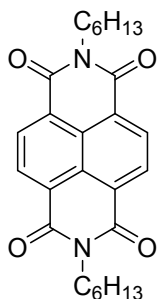
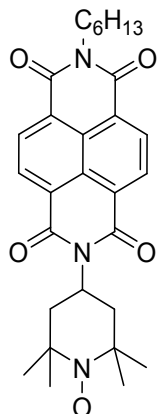


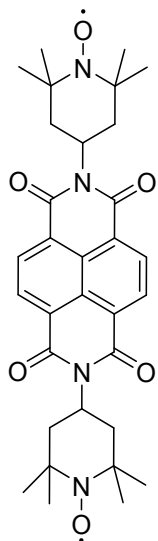
Fig. S1 ^1H NMR spectrum of NDI-0 (600 MHz, CDCl_3).

2,7-dihexylbenzo[*lmn*][3,8]phenanthroline-1,3,6,8(2*H*,7*H*)-tetraone (NDI-0)

Mp 223-224 °C; ^1H NMR (CDCl_3 , 600.0 MHz): δ : 8.76 (s, 4H), 4.19 (t, 4H, J = 7.8 Hz), 1.77-1.72 (m, 4H), 1.46-1.41 (m, 4H), 1.37-1.32 (m, 8H), 0.90 (t, 6H, J = 7.2 Hz).



NDI-1 (124 mg, 37%). Mp 157-158 °C; CW-EPR (CHCl_3): $I = 1$ (^{14}N) and superhyperfine coupling to 12 nuclei with $I = \frac{1}{2}$ (^1H), $g_{iso} = 2.0033$, $\Delta\text{AN} = 44.80$ Hz, $A_H = 1.18$ Hz. ESI HRMS (acetonitrile) m/z calcd. for $\text{C}_{29}\text{H}_{35}\text{N}_3\text{O}_5$ [$\text{M}+\text{H}]^+$: 505.2577, found 505.2546.



NDI-2 (162 mg, 72%). Mp 240-241 °C; CW-EPR (CHCl_3): $I = 1$ (^{14}N) and superhyperfine coupling to 12 nuclei with $I = \frac{1}{2}$ (^1H), $g_{iso} = 2.0033$, $\Delta\text{AN} = 44.80$ Hz, $A_H = 1.18$ Hz. ESI HRMS (acetonitrile) m/z calcd. for $\text{C}_{32}\text{H}_{39}\text{N}_4\text{O}_6$ [$\text{M}+\text{H}]^+$: 575.2870, found 575.2829.

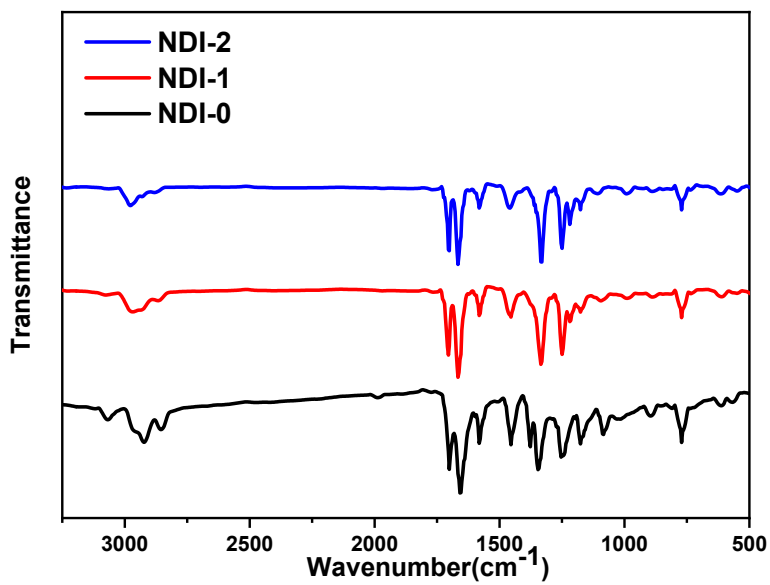


Fig. S2 FTIR spectra of NDI-0, NDI-1, NDI-2.

In the spectra of the NDI-0, NDI-1, NDI-2, the bands at 2969 cm^{-1} , 1658 cm^{-1} , 1581 cm^{-1} and 1335 cm^{-1} are due to C-H, C=O, C=C, C–N stretching vibration modes, respectively. And the band at 1454 cm^{-1} is ascribed to the C-H bending vibration.

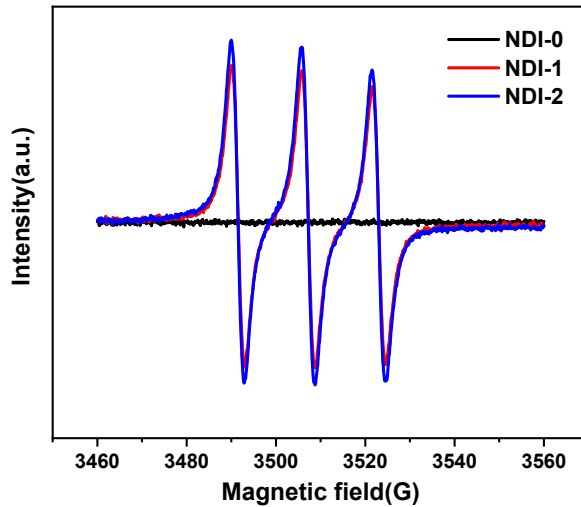


Fig. S3 Steady-state CW EPR spectra of NDI-0, NDI-1, NDI-2 in chloroform solution.

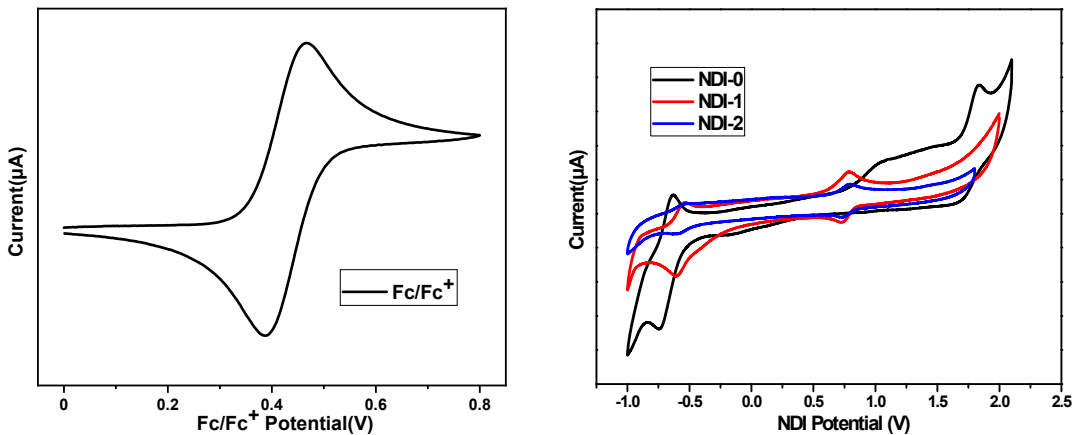


Fig. S4 The CV curves of NDI derivatives.

Cyclic voltammetry (CV) was carried out in nitrogen-purged dichloromethane or acetonitrile solution at r.t. with a CHI voltammetric analyzer. Tetrabutylammonium hexafluorophosphate (0.1 M) was used as the supporting electrolyte. The conventional three-electrode configuration consists of a platinum working electrode, a platinum wire auxiliary electrode, and an Ag/AgCl reference electrode with ferrocenium-ferrocene (Fc^+/Fc) as the internal standard. Cyclic voltammograms were obtained at a scan rate of 100 mV s⁻¹. The onset potential (E_{onset}) was determined from the intersection of two tangents drawn at the rising and background current of the cyclic voltammogram, and the HOMO or LUMO energy levels (eV) of these compounds are caculated according to the formula: $-\left[4.8 \text{ eV} + (E_{\text{onset}}) - E_{1/2(\text{Fc}/\text{Fc}^+)}\right]$.

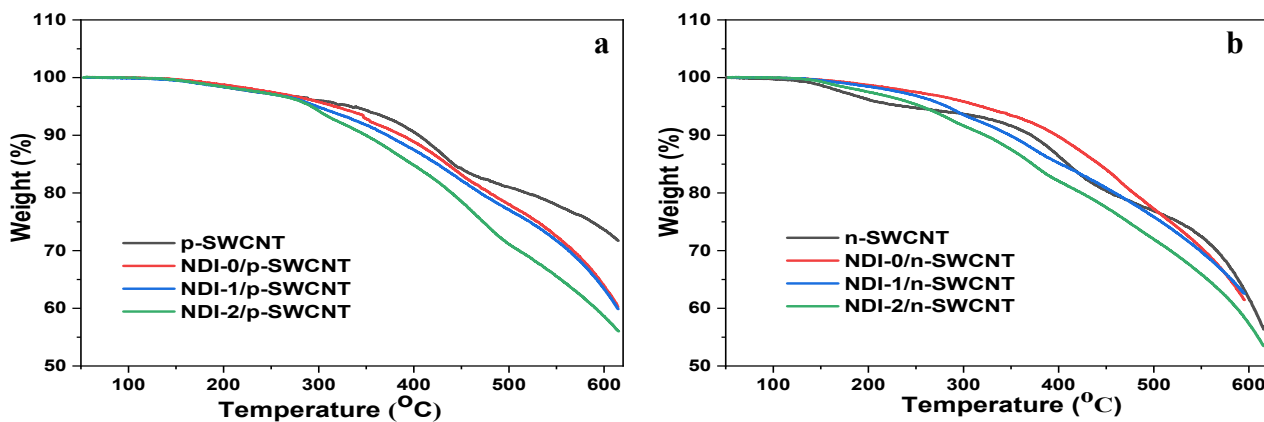


Fig. S5 TGA curves of pristine SWCNTs, and doped SWCNT/NDIs composite films under nitrogen atmosphere: (a) p-type pristine SWCNT and NDIs/p-SWCNT composite films (b) n-type pristine SWCNT and NDIs/n-SWCNT composite films.

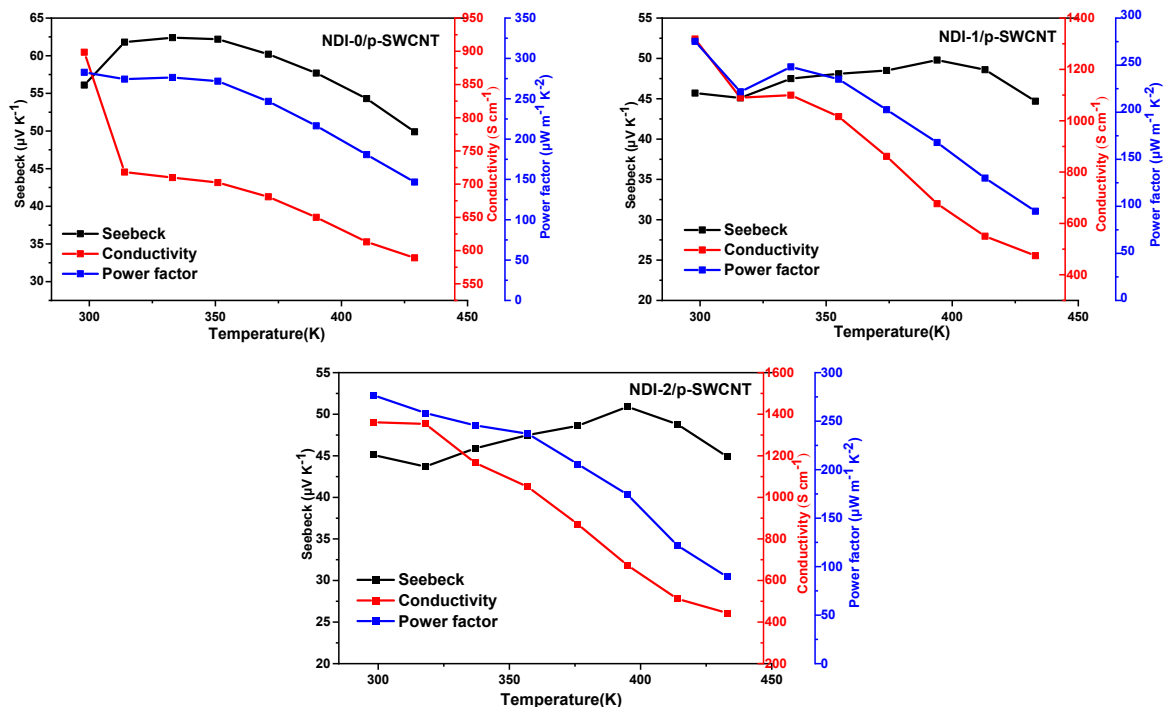


Fig. S6 Temperature (T) dependence of the TE performance of NDI-0/p-SWCNT, NDI-1/p-SWCNT and NDI-2/p-SWCNT (mass ratios: 1:4).

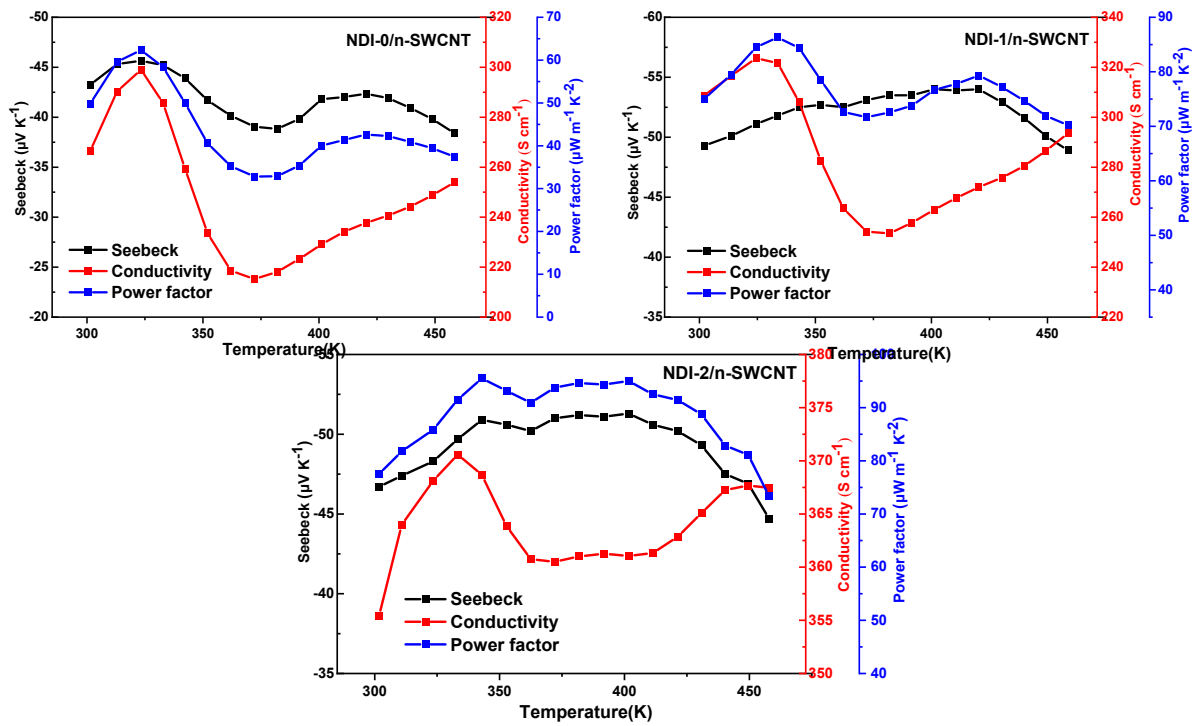


Fig. S7 Temperature (T) dependence of the TE performance of NDI-0/n-SWCNT, NDI-1/n-SWCNT and NDI-2/n-SWCNT (mass ratios: 1:4).

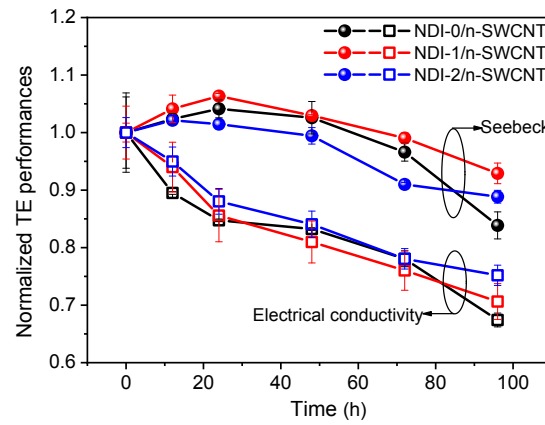


Fig. S8 The air stability of the n-type composites exposed in air.

Table S1 Summary of the thicknesses of different composite films (NDI (0-2)/SWCNT with mass ratios 1:4).

Materials	Thickness (μm)										Average thickness (μm)	Standard deviation (μm)
The pristine p-SWCNT	1.6899	1.6138	1.8534	1.7231	1.6003	1.6285	1.8390	1.7390	1.7534	1.7156	0.0923	
NDI-0/p-SWCNT	1.6029	1.5521	1.7041	1.6873	1.6453	1.6124	1.7102	1.6392	1.7150	1.6521	0.0564	
NDI-1/p-SWCNT	1.6325	1.6269	1.6420	1.6054	1.5360	1.6210	1.6126	1.5891	1.5676	1.6037	0.0341	
NDI-2/p-SWCNT	1.5455	1.6129	1.6414	1.6429	1.6503	1.7356	1.6677	1.6652	1.7111	1.6525	0.0547	
The pristine n-SWCNT	1.8895	1.8647	1.9208	2.2087	1.9401	1.8666	1.8889	1.8855	2.0677	1.9481	0.1159	
NDI-0/n-SWCNT	1.9073	1.9302	1.9323	2.0718	1.8248	1.8322	1.7745	1.8261	1.7975	1.8774	0.0928	
NDI-1/n-SWCNT	1.7275	1.8201	1.9023	1.8975	1.9287	2.1288	1.8494	1.8193	1.7600	1.8704	0.1173	
NDI-2/n-SWCNT	1.9559	1.8872	1.7339	1.9743	1.6687	1.8302	1.8885	1.9067	1.9168	1.8625	0.1016	

We also try to measure the thermal conductivity of the pristine SWCNT and composites by transient plane source method. Because thin films are unable to be measured, the samples are pressing into tablets with a diameter of 10 mm and a height of 2 ~ 4 mm. The thermal conductivity of the tablets ranges approximately $1.14 \sim 1.82 \text{ W m}^{-1} \text{ K}^{-1}$ at 300 K as shown in the following table. We found that the thermal conductivities of p-type composite films are slightly larger than that of the n-type composite films, and the three NDI derivatives exhibit similar thermal conductivities. It worthy noted that the thermal conductivity of the same composite tablets varies greatly with its thickness. The thinner of the tablet sample, the lower of the thermal conductivity. For example, when the thickness is 4.40 mm, the thermal conductivity of NDI-2/n-SWCNT is $1.82 \text{ W m}^{-1} \text{ K}^{-1}$, and when the thickness is 2.89 mm, the thermal conductivity is decreased to $1.39 \text{ W m}^{-1} \text{ K}^{-1}$. Considering the composite films used in this work are only approximately $1.25 \sim 1.95 \mu\text{m}$ thick, we believe the composite films have much smaller thermal conductivity than $1.14 \text{ W m}^{-1} \text{ K}^{-1}$. Even though these results indicate that the composite films indeed have low thermal conductivity, their exact thermal conductivity are still unknown. Therefore, we can only conclude that the composite films have low thermal conductivity and the introduction of radical groups will not greatly change the thermal conductivity of NDI/SWCNT composites. Actually, the

performances of the TE generators can reflect the comprehensive influences of these three parameters (S , σ and κ), indicating radical-containing composite films have superior performances than NDI-0/SWCNT.

Table S2 Thermal conductivity of pristine SWCNT and composites based on transient plane source method

Sample (300K)	Thickness (mm)	Thermal conductivity (W m ⁻¹ K ⁻¹)
p-SWCNT	2.23	1.14
	3.45	1.64
NDI-0/p-SWCNT	2.05	1.58
NDI-1/p-SWCNT	3.65	1.65
NDI-2/p-SWCNT	2.63	1.54
n-SWCNT	4.24	1.75
NDI-0/n-SWCNT	2.45	1.24
NDI-1/n-SWCNT	2.64	1.22
NDI-2/n-SWCNT	2.89	1.39

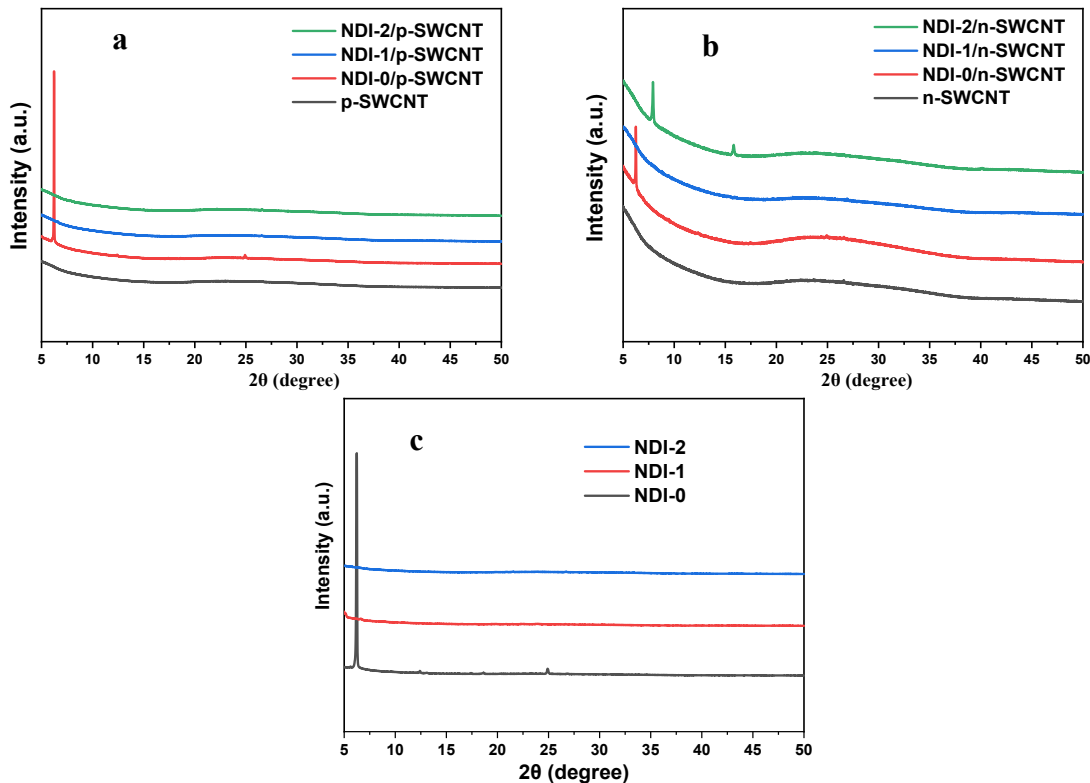


Fig. S8 XRD patterns of pristine SWCNTs, pure NDIs-(0-2), and NDIs/SWCNT composite films (mass ratio: 1/4): (a) p-type pristine SWCNT and NDIs/p-SWCNT composite films (b) n-type pristine SWCNT and NDIs/n-SWCNT composite films. (c) pure NDI-0, NDI-1, NDI-2.

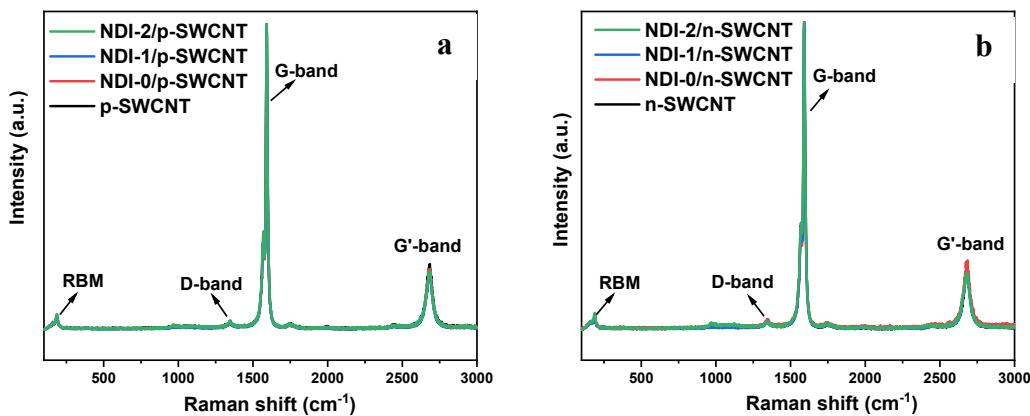


Fig. S9 Raman spectra of the pure SWCNTs and composite films, (a) p-type pristine SWCNT and NDIs/p-SWCNT composite films; (b) n-type pristine SWCNT and NDIs/n-SWCNT composite films.

In order to further study the variation of DOS between SWCNT and NDI derivatives, the UPS measurements of the pristine SWCNT, NDI-1 and NDI-1/p-SWCNT composite films with different mass ratios are obtained as shown in Fig. S10. With increasing the SWCNT loading, clear shifts of high binding energy cutoff and the HOMO onsets towards lower binding energies are observed, indicating a reduction of the hole injection barrier (difference of the Fermi level of SWCNT to the HOMO onset of the NDIs).¹ The density of valence electronic states (DOVS) of NDIs/p-SWCNT can be probed by this UPS (Fig.S10b). A broadening of DOVS of NDI-1/p-SWCNT was clearly noticed, which originated from the interactions between SWCNT and NDI molecules². We have added these discussions in the supporting information.

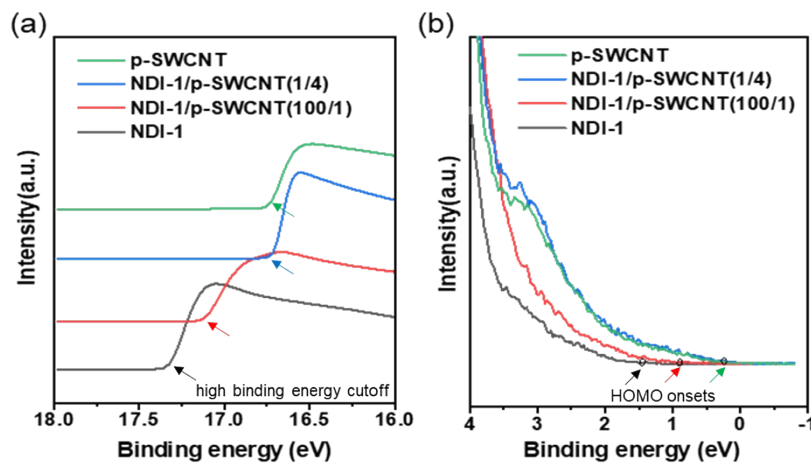


Fig. S10 (a) Secondary electron cutoffs of UPS spectra showing work function changes; (b) low binding-energy region showing the DOVS of pristine SWCNT, NDI-1 and NDI-1/p-SWCNT composite films with different mass ratios.

¹ M. L. Tietze, L. Burtone, .M. Riede, B. Lüssem and K. Leo, *Phys. Rev. B*, 2012, **86**, 035320.

² X. Zhou, C. Pan, C. Gao, A. Shinohara, X. Yin, L. Wang, Y. Li, Q. Jiang, C. Yang and L. Wang, *J. Mater. Chem. A*, 2019, **7**, 10422.

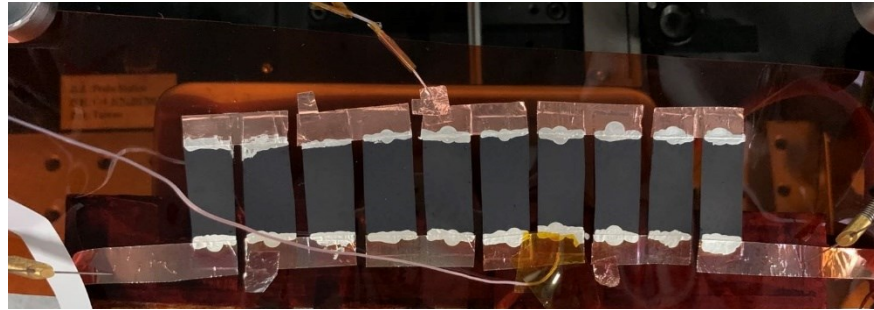


Fig. S11 A photograph of the TE module made up of five couples of p-type and n-type films, where the NDIs/SWCNT composite film was used as both p-type and n-type component.

Table S3 Comparison on TEG performances between our module and literatures

Sample	Device type	TE legs	ΔT (K)	Power (μW)	Power density ($\mu W/cm^2$)	reference
NDI-1/SWCNT (p) NDI-1/SWCNT (n)	p-n	10	33	0.81	115.7	This work
NDI-1/SWCNT (p) NDI-1/SWCNT (n)	p-n	10	45	1.41	201.4	This work
NDI-1/SWCNT (p) NDI-1/SWCNT (n)	p-n	10	65	2.81	401.4	This work
PEDOT:PSS (p) TiS_2 hybrid (n)	p-n	10	70	0.90	250	1
PEDOT:PSS/SWNTs (p) C_{60}/TiS_2 (n)	p-n	4	20	0.335	168	2
SWCNT (p) PEI/SWCNT (n)	p-n	16	49.5	1.16	48.0	3
Te/PEDOT:PSS/ Cu_7Te_4	p	8	39.1	0.095	39.5	4
Te/PEDOT:PSS	p	9	40	0.048	57.2	5
PEDOT:PSS/ Cu_2Se	p	9	30	0.328	91	6

1. R. Tian, C. Wan, Y. Wang, Q. Wei, T. Ishida, A. Yamamoto, A. Tsuruta, W. Shin, S. Li, K. Koumoto, *J. Mater. Chem. A*, 2017, **5**, 564.
2. L. Wang, Z. Zhang, L. Geng, T. Yuan,; Y. Liu, J. Guo, L. Fang, J. Qiu, S. Wang, *Energy Environ. Sci.*, 2018, **11**, 1307.

3. M. Sheng, Y. Wang, C. Liu, Y. Xiao, P. Zhu, Y. Deng, *Carbon*, 2020, **158**, 802.
4. Y. Lu, Y. Qiu, Q. Jiang, K. Cai, Y. Du, H. Song, M. Gao, C. Huang, J. He, D. Hu, *ACS Appl. Mater. Interfaces*, 2018, **10**, 42310.
5. Q. Meng, Q. Jiang, K. Cai, L. Chen, L. Chen, *Org. Electron.*, 2019, **64**, 79.
6. Y. Lu, Y. Ding, Y. Qiu, K. Cai, Q. Yao, H. Song, L. Tong, J. He, L. Chen, *ACS Appl. Mater. Interfaces*, 2019, **11**, 12819.